THE JOURNAL OF PHYSICAL CHEMISTRY C

ARTICLE

pubs.acs.org/JPCC

Anisotropic Thermal Transport in Organic Molecular Crystals from Nonequilibrium Molecular Dynamics Simulations

Dong Wang,[†] Ling Tang,[†] Mengqiu Long,[†] and Zhigang Shuai*[,†,‡]

[†]Key Laboratory of Organic OptoElectronics and Molecular Engineering, Department of Chemistry, Tsinghua University, 100084 Beijing, People's Republic of China

[‡]Key Laboratory of Organic Solids, Beijing National Laboratory for Molecular Science, Institute of Chemistry, Chinese Academy of Sciences, 100190 Beijing, People's Republic of China

ABSTRACT: Nonequilibrium molecular dynamics simulations have been performed to study the anisotropic thermal transport in pentacene crystal. At 300 K, a thermal conductivity of 0.72, 1.1, and 0.61 W/mK is obtained in the direction of reciprocal lattice vectors a^*, b^*, and c^*, respectively, in a perfect crystal with the general Amber force field. The performance of the OPLS-UA force field is also examined, which tends to underestimate the thermal conductivity. Effects of isotopic substitutions and vacancies on the thermal conduction are investigated, and it is found that the conductivity decreases rapidly with the vacancy concentration. Our investigations suggest that classical simulations with well chosen force fields may provide reasonable predictions for the thermal transport properties of organic solids. Such predictions are critical in the determination of thermoelectric figure of merit of materials.

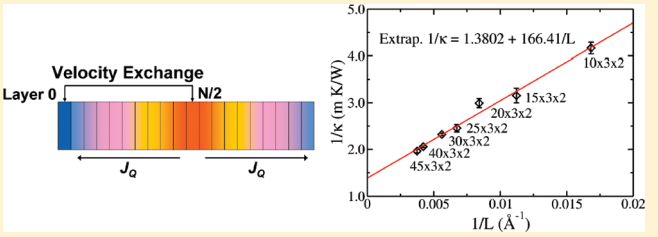

INTRODUCTION

Organic semiconductors constitute the material basis of organic electronic and optoelectronic devices like organic light emitting diodes (OLED), organic field effect transistors (OFET), and organic photovoltaic devices (OPV).[1,2] In these devices, materials with good thermal conducting properties are desirable to avoid thermal degradation. Meanwhile, for thermoelectric applications, materials with very low thermal conductivity are preferred to enhance the thermoelectric efficiency.[3] The thermoelectric efficiency of a material is characterized by the dimensionless thermoelectric figure of merit $zT = S^2\sigma T/\kappa$, where S is the Seebeck coefficient, σ is the electrical conductivity, and κ is the thermal conductivity with contributions from both electrons and lattice vibrations. The electronic thermal conductivity increases with the carrier concentration, as does the electrical conductivity. In not-so-heavily doped semiconductors, the lattice thermal conductivity usually dominates. Lowering the lattice thermal conductivity has been proved an effective way to improve the thermoelectric efficiency. In one earlier work,[4] we studied the electrical transport properties of pentacene based on the first-principles method and the Boltzmann transport theory. To fully characterize the thermoelectric efficiency of a material, accurate determination of the lattice thermal conductivity is required. Currently, both theoretical and experimental studies on the lattice thermal conductivity are scarce for organic solids. The intention of this work is to develop reliable theoretical and computational methods for predicting the lattice thermal conductivity of organic solids.

The methods that can be used to calculate the lattice thermal conductivity fall mainly into two categories. One class of approaches is based on kinetic theories such as the Boltzmann transport equation (BTE).[5] In real materials, phonons are scattered by defects and boundaries, in addition to other phonons due to anharmonic lattice vibrations. Consequently, a limited lifetime or mean free path of phonons is observed. To apply the BTE to extracting the lattice thermal conductivity, such parameters as phonon dispersion relations, phonon density of states, and phonon relaxation times are necessary. However, it is quite challenging to calculate relaxation times because various scattering mechanisms have to be considered explicitly. Molecular dynamics (MD) simulations represent another class of approaches that can be used to obtain the lattice thermal conductivity directly. Besides, parameters required by the BTE, such as phonon dispersion relations and phonon density of states, can be easily derived from these simulations. Given accurate classical force fields developed to describe interactions between atoms, employing MD simulations to extract thermal conductivities is straightforward.

Both equilibrium and nonequilibrium MD simulations have been extensively used to extract the lattice thermal conductivity.[6−13] The equilibrium MD approach is based on the Green−Kubo formalism derived from the linear response theory, in which the thermal conductivity is expressed in terms of heat current correlation functions.[14] The expression for heat current is, however, quite complicated for molecular systems where many-body interactions are present. In the nonequilibrium MD approach, a heat flux across the system is applied, and the

Received: September 14, 2010
Revised: January 10, 2011
Published: March 08, 2011

resulting temperature gradient is measured after the system has established a steady state. The thermal conductivity is then obtained based on Fourier's law:

$$\kappa = -\frac{J}{\nabla T} \quad (1)$$

Different algorithms have been proposed to generate the heat flux, such as the velocity rescaling method of Jund and Jullien,[15] Ikeshoji and Hafskold,[16] and the velocity exchange method of Müller-Plathe and Reith.[17]

Although lots of work has been conducted to extract the lattice thermal conductivity of solids from MD simulations, most of them are focused on atomic crystals such as silicon,[6,18] SiC,[11] diamond,[12] and carbon nanotubes.[19] For organic molecular crystals, well-established force fields such as AMBER, OPLS, and COMPASS exist, but their performance in the calculation of thermal transport properties is not known. In this work, we apply the nonequilibrium MD method to investigating the anisotropic thermal transport in organic molecular crystals. Two force fields, the all-atom general Amber force field (GAFF)[20] and the united-atom OPLS-UA[21,22] force field, are chosen. The effects of isotopic substitutions and vacancies on the thermal conductivity are of particular interest and are thoroughly investigated. These investigations are helpful in the search for new organic thermoelectric materials.

METHODOLOGY

Nonequilibrium MD Method. The Müller-Plathe algorithm[17,23] is used to generate the heat flux in the system. The idea of the algorithm is to exchange velocities between two particles of the same mass in different regions of the simulations box. This induces a temperature gradient in the system. Pentacene is known to form different crystal structures under different conditions. In the current study, the crystal structure of pentacene film grown on SiO_2 is adopted.[24] To apply the nonequilibrium MD method to calculating the thermal conductivity, the primitive cell is first replicated in the direction of three lattice vectors a, b, and c to form a super cell. The super cell, which constitutes the simulation box, has to be enlonged in the direction of heat propagation. As an illustration, a simulation box that is enlonged in the direction of lattice vector a is shown in Figure 1. Periodic boundary conditions are applied in all three dimensions. The simulation box is then divided into $N = 20$ layers along the a axis. Note that the simulation box is triclinic in our case and the division is done parallel to the box faces whose normal is in the direction of a^*, so the heat propagates in the direction of a^*, not a. During the exchange of velocities, the hottest carbon atom in the far left layer (layer 0) and the coldest carbon atom in the middle layer (layer $N/2$) are selected. The velocity swapping is performed every 500 or 1000 steps. Over time, this induces a temperature gradient in the system. The temperature of layer 0, which acts as heat sink, decreases, whereas that of layer $N/2$, which acts as heat source, increases. The heat flux imposed is given by the energy transferred per time and area:

$$J = \frac{1}{2At}\sum_{\text{transfers}}\left(\frac{1}{2}mv_{\text{hot}}^2 - \frac{1}{2}mv_{\text{cold}}^2\right) \quad (2)$$

where A is the cross-sectional area, m is the mass of carbon atom, and t is the length of simulation. Under periodic boundary conditions, energy flows in two directions, so the energy transferred should be divided by 2 in the above equation. After a steady state is established, the local temperature of each layer is calculated from the time average of kinetic energies of the particles in that layer.

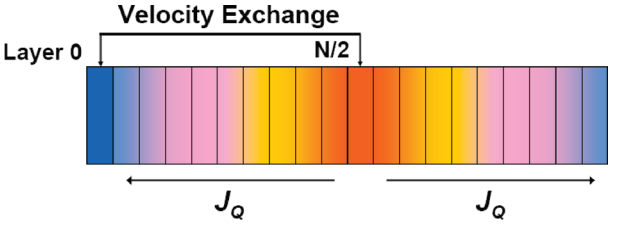

Figure 1. Schematic representation of the simulation box for nonequilibrium MD simulations. Periodic boundary conditions are applied in three dimensions. The box is divided into $N = 20$ bins in the direction of heat conduction. The velocity exchange algorithm of Müller-Plathe has been used for heat flux generation.

Simulation Details. In the simulations, the system is first equilibrated in the NPT ensemble for 500 ps with a temperature of 300 K and a pressure of 1 atm. The box dimensions averaged over the final 300 ps are used in the subsequent nonequilibrium MD simulations. The nonequilibrium simulations last for 5 ns. Typically, 1 ns is long enough to establish a steady temperature profile. The remaining 4 ns is used for time average.

Two sources of errors, arising from the heat current and temperature gradient, give rise to the errors in the thermal conductivity calculated according to eq 1. To estimate the standard deviation of κ, the 4 ns production trajectory is divided into four, each with 1 ns duration. The standard deviation σ is estimated by

$$\sigma^2 = \frac{1}{N-1}(\overline{\kappa^2} - \overline{\kappa}^2) \quad (3)$$

where $N = 4$ is the sample size. The statistical errors can be reduced by perfoming longer simulations. For the OPLS-UA force field, the nonequilibrium MD simulations last for 10 ns, and the initial 5 ns is used for establishing a local thermal equilibrium. The united-atom model consists of less degrees of freedom and no long-range electrostatic interactions, so systems can be simulated for longer times to reduce the statistical errors associated with the thermal fluctuation.

To eliminate finite size effects, simulations have been performed at several system lengths. The thermal conductivity at each finite system length is obtained. An extrapolation procedure, which will be discussed in detail in the next section, is used to extract the thermal conductivity at infinite system length. Throughout this work, initial equilibrations in the NPT ensemble are performed with the GROMACS[25] simulation package, and subsequent nonequilibrium MD simulations are performed with the LAMMPS[26] simulation package. The cutoff for the short-range van der Waals interactions is 10 Å. The long-range electrostatic interactions are treated by the particle mesh Ewald method in GROMACS and Ewald/n method in LAMMPS.

RESULTS AND DISCUSSION

Force Fields, Phonon Density of States, and Heat Capacity. Quite a few empirical force fields have been developed to describe inter- and intramolecular interactions for organic molecules, such as GAFF, OPLS, COMPASS, UFF, and DREIDING. However, these force fields have never been applied to

Table 1. GAFF Parameters Used in the Simulations

bond length	force constant (kcal/mol Å^2)		equilibrium (Å)
C−C	478.4		1.387
C−H	344.3		1.087
bond angle	**force constant (kcal/mol rad^2)**		**equilibrium (deg)**
C−C—C	67.2		119.97
C−C—H	48.5		120.01
dihedral angle	**force constant (kcal/mol)**	**periodicity**	**phase angle (deg)**
X—C−C—X	3.625	2	180
improper	1.1	2	180
van der Waals	**ε (kcal/mol)**		**σ (Å)**
C	0.086		3.4
H	0.015		2.6

studying thermal transport properties of organic solids. In this work, we employ both the GAFF and the OPLS-UA force field in the nonequilibrium simulations to extract the thermal conductivity of pentacene crystal. Two atom types are identified for pentacene in the GAFF: aromatic carbon and aromatic hydrogen. The partial charges of all atoms are derived from the restrained electrostatic potential fit[27,28] at the HF/6-31G* level. The GAFF parameters for all bonded and van der Waals interactions are summarized in Table 1. In the OPLS-UA force field, the carbon atom and the hydrogen atom bonded to it are treated as one united particle, and there are no partial charges on either the united CH atoms or the fused ring carbon atoms. This not only reduces the degrees of freedom in the system, but also removes long-range electrostatic interactions that are computationally costly. For bonded interactions, the parameters of the OPLS-UA force field and the GAFF are similar to each other.

To examine the applicability of these two force fields in the current study, we first use them to calculate the phonon density of states and heat capacity of pentacene. In MD simulations, phonon spectral density can be extracted by suitable analysis of the correlations in the atomic motion. In a solid, phonons associated with wave vectors q are analogous to a set of harmonic oscillators with frequency distribution $f(\omega)$. On the basis of the established theory,[29] the phonon spectral density $f(\omega)$ can be obtained by the Fourier transform of mass-weighted velocity correlation function $c(t)$, which is defined as

$$c(t) = \langle \sum_i m_i v_i(t) v_i(0) \rangle / \langle \sum_i m_i v_i^2(0) \rangle \quad (4)$$

where the summation is over all atoms in the system.

The phonon densities of states obtained with both force fields are shown in Figure 2 for comparison. In the united-atom model, with the removal of C−H stretching motions, peaks in the high frequency region disappear. In the medium frequency region, we can largely identify the correspondence between the peaks for the two force field models, but notable shifts in the frequencies exist. The density of states at low frequencies is highlighted as an inset of Figure 2, which shows little difference in the density of states in the region. The constant volume heat capacity is calculated by

$$C_V = k_B \int d\omega\, f(\omega) \frac{x^2 e^x}{(e^x - 1)^2} \quad (5)$$

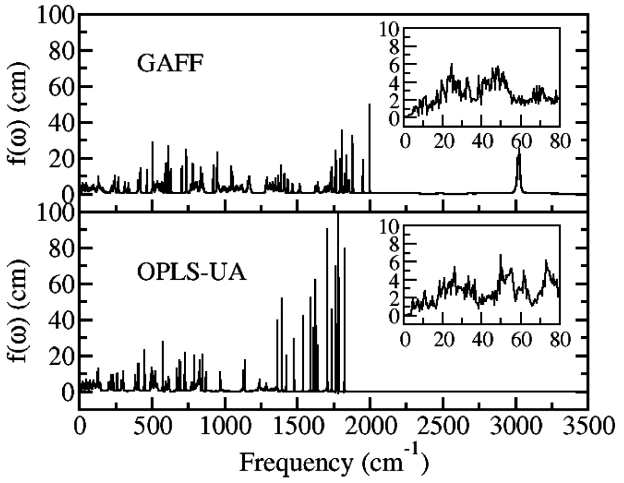

Figure 2. Comparison of phonon density of states calculated with the GAFF (upper panel) and the OPLS-UA (lower panel) force field for pentacene. The inset shows the phonon density of states at low frequencies where the modes are thermally populated. The heat capacity obtained with the two force fields is 272.7 and 250.2 J mol^{-1} K^{-1}, respectively.

with $x = ((\hbar\omega)/(k_B T))$. The molar heat capacity predicted with the GAFF is 272.7 J mol^{-1} K^{-1}. The result obtained with the OPLS-UA force field is lower, 250.2 J mol^{-1} K^{-1}. The low frequency phonons are most relevant for the heat capacity calculation, and the difference between the density of states in the low frequency region is small for the two force field models, so there is only a modest difference in the heat capacity. The heat capacity is also calculated at the B3LYP/6-31G* level of theory with the Gaussian 03 package,[30] and the value is 269.4 J mol^{-1} K^{-1}, which agrees reasonably well with the values calculated with the force fields. The constant pressure heat capacity from the experiment is 311.4 J/(mol K) at 298.9 K.[31] Although both force fields and first-principles calculations have underestimated the heat capacity in comparison with experiment, the agreement is considered reasonable.

It is noted that thermal population of the modes of the system has to be accounted for in the heat capacity calculation. The classical heat capacity calculated from the energy fluctuations in the NVT ensemble is 705.2 J mol^{-1} K^{-1}, which is much larger than the value we report above. The difference between the quantum and classical heat capacities would carry over into the thermal conductivity, because the thermal conductivity is proportional to the heat capacity according to the kinetic theory of thermal conduction. In the studies of thermal transport in proteins based on the kinetic theory,[32−34] the effects of the quantum thermal population of modes on the thermal conductivity have been taken into account. In this work, nonequilibrium MD simulations are used to extract the thermal conductivity directly, and the results are not corrected for the quantum effects. Previous studies have shown that classical simulations do a decent job in many cases with the thermal conductivity calculations,[7,35] even though they substantially overestimate the heat capacity. According to the kinetic theory of heat conduction, the thermal conductivity is not only proportional to the heat capacity, but also limited by the phonon mean free paths and phonon group velocities. One possible explanation for the applicability of classical simulations could be that high frequency phonons that are not populated at 300 K have less significant

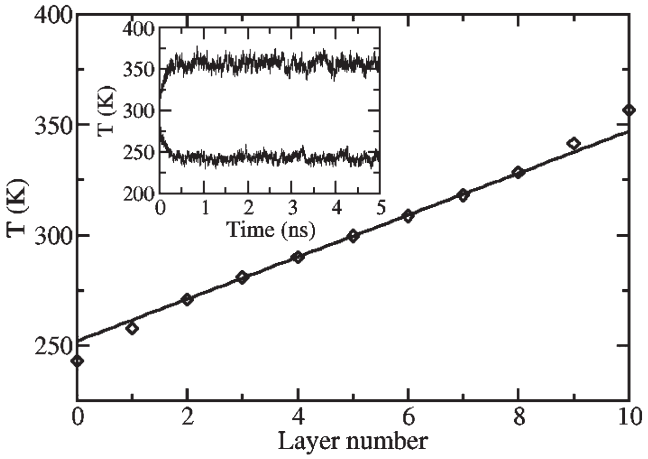

Figure 3. Temperature profile along the *a* axis from nonequilibrium MD simulations for box dimension 40 × 3 × 2. The average has been taken over the final 4 ns of simulation. A linear fit of the data is shown as a solid line. The inset shows temperature evolution with time for both heat sink and heat source.

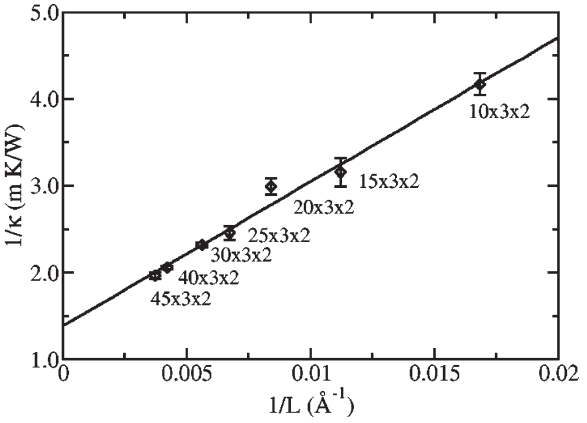

Figure 4. Inverse of the thermal conductivity as a function of inverse of the system length in the direction of *a*. The data points are from the nonequilibrium MD simulations with the GAFF. Linear regression of the data yields the bulk thermal conductivity of pentacene in the direction of *a**, which is 0.72 W/mK in magnitude. The error bars for the thermal resistivity are also shown.

contribution to the thermal conductivity due to short mean free paths and small group velocities.

Anisotropic Thermal Transport. We know that charge transport is anisotropic in organic molecular crystals where molecular packings vary significantly in different crystal directions. Both theoretical[4,36] and experimental[37] studies reveal that the electrical conductivity of pentacene in the direction of the *a* axis is about 2 orders of magnitude larger than that along the *c* axis. Similarly, an anisotropic phonon transport is anticipated in organic molecular crystals. Here, thermal conductivities in three major crystal directions are calculated in a perfect crystal of pentacene with the nonequilibrium MD method and the GAFF as described in the Methodology section.

An example of the temperature profile obtained in the direction of the *a* axis is shown in Figure 3. The profile is essentially linear, except for the region near the heat sink (layer 0) and the heat source (layer 10). The temperature dropoff at the heat sink and pickup at the heat source are caused by the unphysical exchange of momentum between the two layers during the MD run, which is not well balanced by the physical heat flow. The temperature gradient can be obtained by linear regression of the data in the linear region of the profile.

A heat flux on the order of 10^{10} W/m^2 is often applied in the nonequilibrium MD simulations, and a huge thermal gradient is observed. The concern here is that if the temperature difference between adjacent layers is too small relative to the thermal fluctuation in the system, it will be difficult to obtain converged results during reasonable simulation times. Although it has been questioned whether linear response theory holds under such extreme thermal loading, previous studies[6,7] show that the nonequilibrium MD method, when applied appropriately, can give reasonable thermal conductivities that are comparable to those extracted from the Green−Kubo relation in the equilibrium MD simulations and to those measured in the experiments. The linear response region is tested in this work by exchanging the velocities every 200, 500, and 1000 steps, and the induced heat flux changes accordingly. The computed thermal conductivity is found to be independent of the heat flux. In the following simulations, the velocity swapping is performed every 1000 or 500 steps.

An issue associated with the nonequilibrium MD approach is that the calculated thermal conductivity depends strongly on the box length in the direction of heat propagation. This size effect, arising from phonon scatterings at the boundaries of the simulation box, is usually nonnegligible and can only be corrected by the extrapolation procedure.[6,35] According to the kinetic theory of thermal conduction, the thermal conductivity of an isotropic system can be expressed as

$$\kappa = \frac{1}{3}\frac{C_v}{V} vl = \frac{1}{3}\rho c_v v^2 \tau \qquad (6)$$

where C_v and c_v are the constant-volume and specific heat capacities, respectively, V is the volume, ρ is the mass density, τ is the phonon relaxation time, and v and l are the effective phonon velocity and mean free path, respectively. If we assume that phonon scatterings at the box boundaries act independently from scatterings in the true bulk crystal, the phonon relaxation time from the MD simulations can be decomposed into[35]

$$\tau_{MD}^{-1} = \tau_{bulk}^{-1} + \tau_{box}^{-1} \qquad (7)$$

with $\tau_{box}^{-1} = ((v)/(L/2))$ and L as the box length. The thermal conductivity obtained from the MD simulations is then related to the size of the simulation box by[6,35]

$$\frac{1}{\kappa_{MD}} = \frac{3}{\rho c_v v^2}\tau_{MD}^{-1} = \frac{3}{\rho c_v v^2}\left(\tau_{bulk}^{-1} + \frac{2v}{L}\right) \equiv A + \frac{B}{L} \qquad (8)$$

To extract the thermal conductivity for a true bulk system, simulations at several box lengths are performed. The linear dependence of the inverse of thermal conductivity on the inverse of box length is confirmed by the simulation data, as shown in Figure 4. Linear extrapolation of the data gives a thermal conductivity of 0.72 W/mK in the direction of *a**. The effective phone mean free path can be extracted from the extrapolation procedure as $l_{bulk} = v\tau_{bulk} = B/2A$, which gives the value of 60.3 Å in the direction of *a**. The thermal conductivities in the other two crystal directions *b** and *c** are 1.1 and 0.61 W/mK, respectively. The corresponding phonon mean free paths are 392.6 and 42.3 Å. The data points used for the extrapolation are summarized in Table 2. The magnitude of the thermal conductivity in the

dx.doi.org/10.1021/jp108739c |*J. Phys. Chem. C* 2011, 115, 5940–5946

Table 2. Thermal Conductivity and Standard Deviation Obtained at Different Box Lengths

L_b (cells)	10	12	16	20
κ (W/mK)	0.0972	0.1147	0.1534	0.1743
σ (W/mK)	0.0039	0.0028	0.0025	0.0062
L_a = 4 cells and L_c = 2 cells			κ_{bulk} = 1.1 W/mK	

L_c (cells)	6	8	10	12	14	16
κ (W/mK)	0.3161	0.3791	0.3682	0.4343	0.4371	0.4552
σ (W/mK)	0.0083	0.0075	0.0118	0.0224	0.0098	0.0151
L_a = 4 cells and L_b = 3 cells				κ_{bulk} = 0.61 W/mK		

pentacene crystal exhibits an order of $b^* > a^* > c^*$. This order of magnitude for the thermal conductivity is consistent with the order for the electrical conductivity, except that an anisotropy of two is found for the former, whereas an anisotropy of 2 orders of magnitude is found for the latter.

Experiments have been conducted to measure the thermal transport properties for thin films of pentacene and two other organic semiconductors.[38] A conductivity of 0.51 W/mK was determined for pentacene in the direction perpendicular to the film plane. Our calculations predict a thermal conductivity of 0.61 W/mK in the direction of c^*, which agrees reasonably well with the experimental value. The statistical errors associated with our simulations are estimated to be ~5%, and extrapolation to the infinite-size limit tends to magnify statistical errors. Studies have shown that the simulation method can result in errors in the 15−20% range.[7] Meanwhile, the calculations are performed for a perfect crystal where phonon−phonon interactions are the only mechanism of phonon scatterings. When making comparisons with the experimental value, defect and boundary scatterings in real materials have to be taken into account. The effect of defects on the thermal conductivity will be discussed in next subsection.

In comparison with the GAFF, simulations with the OPLS-UA force field predict a conductivity of 0.41, 0.73, and 0.33 W/mK, respectively, in the direction of a^*, b^*, and c^*. Apparently, the thermal conductivity has been systematically underestimated with the OPLS-UA force field. It is noted that in the united-atom representation not only C−H stretching motions are removed, but also those medium frequency modes involving hydrogen atoms disappear, for instance, the H−C−C bending motions at about 1000 cm^{-1}. Because phonons with lower frequencies have longer mean free paths and larger velocities, according to eq 6, lower frequency phonons play a more significant role in the thermal conduction; therefore, removal of these modes can lead to underestimation of the thermal conductivity. One other difference between the all-atom GAFF and the united-atom OPLS-UA force field is that no long-range electrostatic interactions exist in the latter. This discrepancy of the force field can also cause deviation in the extracted thermal conductivity.

Effect of Defects. At room temperature, phonon scattering due to anharmonic lattice vibrations is the major cause of the limited phonon lifetimes and thermal conductivity, whereas at low temperatures defects scattering may become dominant. We consider here two types of defects, isotopic substitutions and vacancies. The thermal conductivity of pentacene containing the 1.1% natural abundance of ^{13}C is calculated with the nonequilibrium MD method and the GAFF. The substitution sites of ^{13}C are chosen randomly. Simulations have been performed for box dimensions of 10, 15, 20, 25, 30, and 40 cells in the direction of a. Figure 5 shows the inverse of thermal conductivity versus the inverse of box length for 1.1% ^{13}C and pure ^{12}C pentacene. A general trend observed is that the thermal conductivity for pentacene with natural abundance ^{13}C is slightly lower than that for pure ^{12}C at the same box length. The extrapolated thermal conductivity for 1.1% ^{13}C is 0.70 W m^{-1} K^{-1}, in comparison with 0.72 W m^{-1} K^{-1} for pure ^{12}C. The results indicate that the isotopic effect is too little to be accurately determined with the current calculations. It has been found that the ratio of thermal conductivity for pure ^{12}C with respect to that for 1.1% ^{13}C for diamond is 1.45 ± 0.16 from the equilibrium MD simulations.[12] Our results suggest that the thermal conductivity of pentacene is much less sensitive to the isotopic substitution than is diamond.

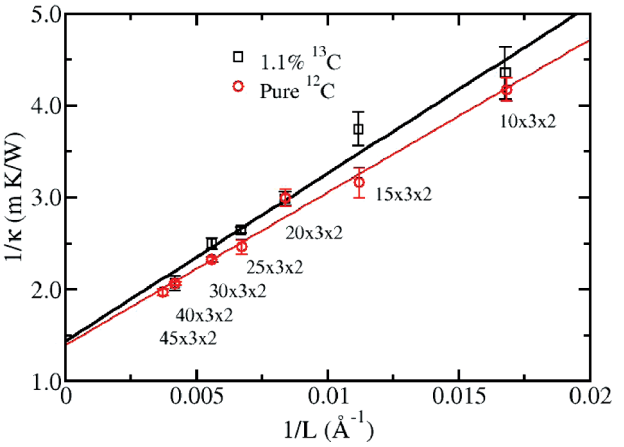

Figure 5. Effect of isotopic substitution. Inverse of the thermal conductivity is shown versus inverse of the box length for both pure ^{12}C pentacene and 1.1% ^{13}C pentacene. The box length is 10, 15, 20, 25, 30, and 40 cells, respectively, in the direction of a.

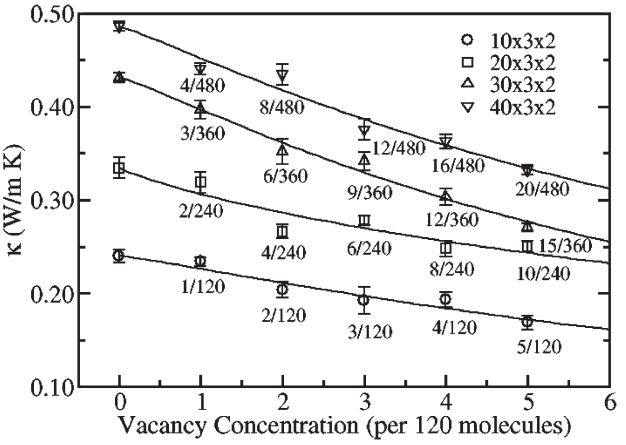

Figure 6. Thermal conductivity of pentacene containing random distributions of vacancies. The solid line represents fitting of the data to function eq 11, with the scaling factor α of 1.16, 0.94, 1.16, and 1.11, respectively, for the box length of 10, 20, 30, and 40 cells in the direction of a.

As a second application, the effects of vacancies on the thermal conductivity are studied. The box dimensions of 10, 20, 30, and 40 cells, respectively, in the direction of a and a random distribution of vacancies are considered. The results in Figure 6 show that the thermal conductivity at fixed box length decreases rapidly with the vacancy concentration, n_v. Assuming that vacancy

scattering is independent of phonon scattering in a perfect crystal, the total phonon scattering time can be decomposed into

$$\tau_{tot}^{-1} = \tau_{perf}^{-1} + \tau_{vac}^{-1} \quad (9)$$

where τ_{perf} is the phonon scattering time in a perfect crystal and τ_{vac} is the scattering time induced by vacancies. If we assume that the phonon velocity and heat capacity are not affected by the vacancies, the thermal conductivity can be written as

$$\kappa_{tot}(n_v) = \frac{\kappa_{perf}}{1 + \kappa_{perf}/\kappa_{vac}} \quad (10)$$

Following the practice of ref 12 the results in Figure 6 are fitted by eq 10 with

$$\kappa_{tot}(n_v) = \frac{\kappa_{perf}}{1 + Cn_v^{\alpha}} \quad (11)$$

and the scaling factor α = 1.16, 0.94, 1.16, and 1.11 is obtained for the box length of 10, 20, 30, and 40 cells, respectively. The fit in eq 11 suggests that the vacancy contribution to the thermal conductivity obeys a scaling law of

$$\kappa_{vac} \propto n_v^{-\alpha} \quad (12)$$

The scaling factor for pentacene is larger than that found for diamond (~0.7),[12] which indicates that the thermal conductivity of pentacene is more sensitive to vacancies than diamond. Finally, it is not clear whether the thermal conductivity is affected by different positions of the defects. The influence of distributions of the defects is not studied in this work.

Thermoelectric Figure of Merit. The thermoelectric properties of pentacene have drawn great attention recently. The Seebeck coefficient,[39] the thermal conductivity,[38] and the power factor[40] of pentacene thin films have been measured experimentally, with the values being 0.3−1 mV/K, 0.51 W/mK, and 2.0 μW/mK^2, respectively. As mentioned earlier, the thermoelectric figure of merit of a material is determined by its Seebeck coefficient S, electrical conductivity σ, and thermal conductivity κ with contributions from both electrons and phonons. In our previous study, the electrical transport properties of pentacene have been calculated on the basis of the first-principles method. However, to evaluate the thermoelectric figure of merit of a material, accurate lattice thermal conductivity is necessary. In particular, it should be kept in mind that in organic molecular crystals both electrical and thermal transport are anisotropic. The motivation of the current work is to examine the anisotropic thermal transport in the crystal of pentacene and its influence on the anisotropic thermoelectric performance of pentacene. The experimentally determined thermal conductivity of pentacene is 0.51 W/mK, which is in the direction perpendicular to the plane of thin films, that is, in the direction of c^*. This value was used in our earlier work to estimate the dimensionless thermoelectric figure of merit in the direction of b, in which direction the thermoelectric figure of merit is the largest among two other crystal directions. Our previous estimation falls into the range of 0.8−1.1.[4] In the current work, we have obtained the lattice thermal conductivity of pentacene in three major crystal directions. The conductivity in the direction of b^* is predicted to be 0.72 W/mK. Accordingly, the upper limit of thermoelectric figure of merit is redefined, which gives the range of 0.5−0.8. Combining our results of both electrical and thermal transport studies of pentacene, we have come to a conclusion that the anisotropy of charge transport is more exaggerated than that of thermal transport, which leads to the best thermoelectric performance in the crystal direction of b and the poorest in the direction of c.

CONCLUSIONS

The heat conduction in pentacene crystal has been investigated by the nonequilibrium MD simulations. The performance of two force fields, the GAFF and the OPLS-UA force field, has been examined. Better agreement between theory and experiment is found with the simulations that use the all-atom model than the united-atom model. Simulations with the OPLS-UA force field tend to underestimate the thermal conductivity of pentacene. The lack of long-range electrostatic interactions in the OPLS-UA force field and less degrees of freedom in the united-atom model are probably the cause of its poorer performance in the prediction of thermal conductivity of pentacene.

The thermal conductivity has been calculated in three major crystal directions. The largest conductivity is found in the direction of b^*. The anisotropy essentially arises from different molecular arrangements and interactions in different crystal directions of organic molecular crystals. In contrast to the anisotropy of 2 orders of magnitude for the electrical conductivity, an anisotropy of two is predicted for the thermal conductivity. The effects of defects on the thermal conductivity have been studied. Two types of defects, isotopic substitutions and vacancies, are considered. It is found that vacancies dramatically decrease the thermal conductivity, and its contribution can be described by a scaling law of $n_v^{-\alpha}$.

Overall, our investigations suggest that molecular dynamics simulations with accurate force field can provide reasonable predictions for the thermal conductivity of organic molecular crystals. Such calculations can be very useful in the determination of thermoelectric figure of merits, and in the search for new thermoelectric materials.

AUTHOR INFORMATION

Corresponding Author
*E-mail: zgshuai@tsinghua.edu.cn.

ACKNOWLEDGMENT

This work is supported by the National Science Foundation of China (grant nos. 20833004, 20773145, 20733006, and 20903060). Computational resources are provided by the Supercomputing Center of the Chinese Academy of Sciences.

REFERENCES

(1) Forrest, S. R. *Nature* **2004**, *428*, 911.
(2) Shakouri, A. *Proc. IEEE* **2006**, *94*, 1613.
(3) Mahan, G.; Sales, B.; Sharp, J. *Phys. Today* **1997**, *50*, 42.
(4) Wang, D.; Tang, L.; Long, M. Q.; Shuai, Z. G. *J. Chem. Phys.* **2009**, *131*, 224704.
(5) Srivastava, G. P. *The Physics of Phonons*; Adam Hilger: Bristol, 1990.
(6) Schelling, P. K.; Phillpot, S. R.; Keblinski, P. *Phys. Rev. B* **2002**, *65*, 144306.
(7) Zhou, X. W.; Aubry, S.; Jones, R. E.; Greenstein, A.; Schelling, P. K. *Phys. Rev. B* **2009**, *79*, 115201.
(8) Wang, Z. G.; Zu, X. T.; Gao, F.; Weber, W. J.; Crocombette, J. P. *Appl. Phys. Lett.* **2007**, *90*, 161923.

(9) Che, J. W.; Cagin, T.; Goddard, W. A. *Nanotechnology* **2000**, *11*, 65.
(10) Schelling, P. K.; Phillpot, S. R.; Keblinski, P. *J. Appl. Phys.* **2004**, *95*, 6082.
(11) Li, J.; Porter, L.; Yip, S. *J. Nucl. Mater.* **1998**, *255*, 139.
(12) Che, J. W.; Cagin, T.; Deng, W. Q.; Goddard, W. A. *J. Chem. Phys.* **2000**, *113*, 6888.
(13) Volz, S. G.; Chen, G. *Phys. Rev. B* **2000**, *61*, 2651.
(14) Kubo, R.; Toda, M.; Hashitsume, N. *Statistical Physics II*; Springer: Berlin, 1985.
(15) Jund, P.; Jullien, R. *Phys. Rev. B* **1999**, *59*, 13707.
(16) Ikeshoji, T.; Hafskjold, B. *Mol. Phys.* **1994**, *81*, 251.
(17) Müller-Plathe, F.; Reith, D. *Comput. Theor. Polym. Sci.* **1999**, *9*, 203.
(18) Donadio, D.; Galli, G. *Phys. Rev. Lett.* **2009**, *102*, 195901.
(19) Donadio, D.; Galli, G. *Phys. Rev. Lett.* **2007**, *99*, 255502.
(20) Wang, J. M.; Wolf, R. M.; Caldwell, J. W.; Kollman, P. A.; Case, D. A. *J. Comput. Chem.* **2004**, *25*, 1157.
(21) Jorgensen, W. L.; Madura, J. D.; Swenson, C. J. *J. Am. Chem. Soc.* **1984**, *106*, 6638.
(22) Jorgensen, W. L.; Tirado-Rives, J. *Proc. Natl. Acad. Sci. U.S.A.* **2005**, *102*, 6665.
(23) Müller-Plathe, F. *J. Chem. Phys.* **1997**, *106*, 6082.
(24) Schiefer, S.; Huth, M.; Dobrinevski, A.; Nickel, B. *J. Am. Chem. Soc.* **2007**, *129*, 10316.
(25) Hess, B.; Kutzner, C.; van der Spoel, D.; Lindahl, E. *J. Chem. Theory Comput.* **2008**, *4*, 435.
(26) Plimpton, S. *J. Comput. Phys.* **1995**, *117*, 1.
(27) Bayly, C. I.; Cieplak, P.; Cornell, W. D.; Kollman, P. A. *J. Phys. Chem.* **1993**, *97*, 10269.
(28) Cornell, W. D.; Cieplak, P.; Bayly, C. I.; Kollman, P. A. *J. Am. Chem. Soc.* **1993**, *115*, 9620.
(29) Dickey, J. M. *Phys. Rev.* **1969**, *188*, 1407.
(30) Frisch, M. J.; Trucks, G. W.; Schlegel, H. B.; Scuseria, G. E.; Robb, M. A.; Cheeseman, J. R.; Montgomery, J. A., Jr.; Vreven, T.; Kudin, K. N.; Burant, J. C.; Millam, J. M.; Iyengar, S. S.; Tomasi, J.; Barone, V.; Mennucci, B.; Cossi, M.; Scalmani, G.; Rega, N.; Petersson, G. A.; Nakatsuji, H.; Hada, M.; Ehara, M.; Toyota, K.; Fukuda, R.; Hasegawa, J.; Ishida, M.; Nakajima, T.; Honda, Y.; Kitao, O.; Nakai, H.; Klene, M.; Li, X.; Knox, J. E.; Hratchian, H. P.; Cross, J. B.; Bakken, V.; Adamo, C.; Jaramillo, J.; Gomperts, R.; Stratmann, R. E.; Yazyev, O.; Austin, A. J.; Cammi, R.; Pomelli, C.; Ochterski, J. W.; Ayala, P. Y.; Morokuma, K.; Voth, G. A.; Salvador, P.; Dannenberg, J. J.; Zakrzewski, V. G.; Dapprich, S.; Daniels, A. D.; Strain, M. C.; Farkas, O.; Malick, D. K.; Rabuck, A. D.; Raghavachari, K.; Foresman, J. B.; Ortiz, J. V.; Cui, Q.; Baboul, A. G.; Clifford, S.; Cioslowski, J.; Stefanov, B. B.; Liu, G.; Liashenko, A.; Piskorz, P.; Komaromi, I.; Martin, R. L.; Fox, D. J.; Keith, T.; Al-Laham, M. A.; Peng, C. Y.; Nanayakkara, A.; Challacombe, M.; Gill, P. M. W.; Johnson, B.; Chen, W.; Wong, M. W.; Gonzalez, C.; Pople, J. A. *Gaussian 03*, revision E.01; Gaussian, Inc.: Wallingford, CT, 2004.
(31) Fulem, M.; Lastovka, V.; Straka, M.; Ruzicka, K.; Shaw, J. M. *J. Chem. Eng. Data* **2008**, *53*, 2175.
(32) Nguyen, P. H.; Park, S. M.; Stock, G. *J. Chem. Phys.* **2010**, *132*, 025102.
(33) Yu, X.; Leitner, D. M. *J. Phys. Chem. B* **2003**, *107*, 1698.
(34) Yu, X.; Leitner, D. M. *J. Chem. Phys.* **2005**, *122*, 054902.
(35) Jiang, H.; Myshakin, E. M.; Jordan, K. D.; Warzinski, R. P. *J. Phys. Chem. B* **2008**, *112*, 10207.
(36) Cheng, Y. C.; Silbey, R. J.; da Silva, D. A.; Calbert, J. P.; Cornil, J.; Bredas, J. L. *J. Chem. Phys.* **2003**, *118*, 3764.
(37) Jurchescu, O. D.; Baas, J.; Palstra, T. T. M. *Appl. Phys. Lett.* **2004**, *84*, 3061.
(38) Kim, N.; Domercq, B.; Yoo, S.; Christensen, A.; Kippelen, B.; Graham, S. *Appl. Phys. Lett.* **2005**, *87*, 241908.
(39) Pernstich, K. P.; Rossner, B.; Batlogg, B. *Nat. Mater.* **2008**, *7*, 321.
(40) Harada, K.; Sumino, M.; Adachi, C.; Tanaka, S.; Miyazaki, K. *Appl. Phys. Lett.* **2010**, *96*, 253304.